Supporting Information

Selective C_{2+} Alcohol Synthesis from Direct CO_2 Hydrogenation over a Cs-Promoted Cu-Fe-Zn Catalyst

Di Xu[1], Mingyue Ding[2], Xinlin Hong[1*], Guoliang Liu[1*], and Shik Chi Edman Tsang[3]

[1] College of Chemistry and Molecular Sciences, Wuhan University, Wuhan 430072, China

[2] School of Power and Mechanical Engineering, Wuhan University, Wuhan 430072, China

[3] Wolfson Catalysis Centre, Department of Chemistry, University of Oxford, Oxford, OX1 3QR, UK.

***Corresponding authors:**

Email address: hongxl@whu.edu.cn; liugl@whu.edu.cn

Experimental Section

Catalyst preparation. Mixed CuFeZn oxides were prepared by using a coprecipitation method. In detail, the CuFeZn precipitates were obtained by a precipitation of Cu, Zn and Fe nitrate solution (0.2 mol L^{-1}) using aqueous $(NH_4)_2CO_3$ (0.24 mol L^{-1}) as the precipitating agent with a single-drop method at 70 ºC and pH = 9 under stirring. The molar ratio of Cu:Fe:Zn was set at x:y:1. The products were collected by centrifugation and washed with deionized water for several times, followed by drying at 80 ºC for 12 h. After calcination at 400 ºC for 2 h, the CuFeZn ternary metal oxides were obtained. Cs modified CuFeZn catalysts were prepared by impregnating CuFeZn oxides (1 g) in a Cs_2CO_3 aqueous solution, followed by drying at 110 ºC and calcination at 400 ºC for 2 h. The final catalysts are denoted as x%Cs-$C_yF_zZ_{1.0}$, where x% represents the weight percent of Cs and $C_yF_zZ_{1.0}$ represents Cu, Fe and Zn with a molar ratio of y:z:1.0. And the weight percent of Cs is fixed at 3% if it is not marked.

Catalyst characterization. All samples were reduced under 10% H_2/Ar flow at 350 ºC prior to characterization. After cooling down to room temperature, the samples were transferred into a sample vial of liquid chromatography and we then replaced the air in the bottle with N_2. The bottle was then put into a Teflon flask containing Fe powder at the bottom and then vacuumed and filled with N_2 to purge O_2 in the flask.

Transmission Electron Microscopy (TEM) images were acquired on a JEM-2100F (JEOL) at 200 kV. After taken out from sample vial filled with protective N_2, the sample was dispersed in ethanol and then deposited on a carbon film. The TEM imaging was

immediately performed after ethanol volatilization. The lattice d-spacing was measured with Digital Micrograph software as follows: we first drew a line vertical to lattice fringes, and then we generally counted 10-20 units of fringes to calculate the d-spacing value. N_2 sorption was used to analyze Brunauer-Emmett-Teller (BET) surface area and pore volume on an ASAP 2020 (Micromeritics). Powder X-ray diffraction (PXRD) was performed on a Bruker D8 Advances with Cu Kα radiation. The samples were scanned from 20° to 60° with a step angle of 0.02°. The crystallite size was calculated with Scherrer formula. Elemental analysis was detected by ICP-AES with a ContrAA 700 spectrometer (Analytikjena).

H_2 temperature-programmed reduction (TPR) experiments were performed on Micromeritics Autochem 2920. The experimental procedure is described as follows: 50 mg sample was loaded on the layer of quartz wool in a U-shaped quartz tube and then heated to 150 ºC with a rate of 4 ºC min^{-1} in an Ar flow (30 mL min^{-1}) for 0.5 hour to clean the sample. The experiment was carried out in a 5% H_2/Ar flow of 30 mL min^{-1} with heating to 600 ºC at a heating rate of 10 ºC min^{-1}. The signal was recorded by a TCD detector.

H_2 temperature-programmed desorption (TPD) experiments were performed as follows: 100 mg sample was reduced under 5% H_2/Ar flow (30 mL/min) at 350 ºC for 1 h and cooled down to 50 ºC. Then, the gas was switched to Ar at a flow rate of 50 mL/min to purge the residual H_2 for 20 min. After that, the TPD measurements were conducted from 50 ºC to 600 ºC with a TCD detector.

CO_2 temperature-programmed desorption (TPD) experiments were carried out as follows: 100 mg sample was reduced under 5% H_2/Ar flow (30 mL/min) at 350 ºC for 1 h. Then, the gas was switched to Ar at a flow rate of 30 mL/min to purge the residual H_2 and cooled down to 50 ºC. After a pre-adsorption of CO_2 in 30 mL min^{-1} flow at 50 ºC, the gas was switched to Ar at a flow rate of 50 mL min^{-1} to purge the residual CO_2. The TPD measurements were conducted by using He as carrier from 50 ºC to 600 ºC with a quadrupole mass spectrometer (Hidden, QIC-20) detector.

Temperature-programmed surface reaction (TPSR) experiments were performed as follows: 50 mg sample was reduced in a 5% H_2/Ar atmosphere at 350 ºC for 1 hour and cooled down to 50 ºC in 30 mL min^{-1} of Ar. After a pre-adsorption of CO in 30 mL min^{-1} flow at 50 ºC, the gas was switched to Ar at a flow rate of 50 mL min^{-1} to purge the residual CO. The TPSR experiments were begun by using 5% H_2/Ar as carrier from 50 ºC to 700 ºC (10 ºC min^{-1}) with a quadrupole mass spectrometer (Hidden, QIC-20) detector. The m/q of desorption species are listed as follows: H_2 (2), H_2O (18), CO_2 (44), CH_4 (16) and CO (28).

In situ diffuse reflectance Fourier transform infrared spectroscopy (DRIFTS) measurements were accomplished in an in situ reaction cell on a Bruker VERTEX 70 spectrometer with a MCT detector. The DRIFTS tests were carried out at 100 ºC and 200 ºC in a H_2/CO_2 (3:1) flow of 30 mL min^{-1} at a total pressure of 0.3 MPa. The sample was reduced at 350 ºC in a 10% H_2/Ar flow of 30 mL min^{-1} for 1 h, and then purged with Ar at the same temperature for 1 h before test. The spectra were collected by 32

scans at a resolution of 4 cm^{-1}. Each spectrum was referenced to the spectrum collected at the same temperature in Ar flow. The background spectra were obtained after cooling down to the desired temperature.

Catalytic testing. The HAS from CO_2 hydrogenation was evaluated on a customized fixed-bed reactor (internal diameter of 10 mm). 0.2 g catalyst was diluted with 0.4 g quartz sand and then loaded into a stainless steel tube. Before measurement, the catalyst was reduced at 350 ^{o}C for 1 h in a 10% H_2/Ar flow of 30 mL min^{-1}. After cooling down to room temperature, the feeding gas with a $H_2/CO_2/N_2$ (N_2 as internal standard) ratio of 72/24/4 was introduced into the reactor and then pressurized to 5 MPa. Then the gas flow was set as 15 mL min^{-1} and the reaction temperature was raised up to the desired temperature with a heating rate of 5 ºC min^{-1}. The post-reactor line and valves were maintained at 150 ºC to avoid product condensation. The products were analyzed online by a gas chromatograph equipped with thermal conductivity detector (TCD) and flame ionization detector (FID). CO_2 conversion was calculated using an internal standard method and product selectivity was calculated on a molar carbon basis. All data were obtained after the reaction lasts for 3 h at each temperature for the equilibrium of tail gas composition. Then the reaction temperature was continuously increased to higher temperatures to obtain other catalytic data with using the same catalysts. For the time on stream test, the reaction was kept at 310 ºC. As for the referenced Cs-CxFyZ1 sample reduced by syngas, the pre-reduction treatment was performed at 350 ºC for 5 h in 10% H_2/Ar flow of 15 mL min^{-1} and 5% CO/Ar flow of 15 mL min^{-1}.

The methanol steam reforming experiment was performed on another fixed-bed reactor (internal diameter of 8 mm) equipped with a high-pressure constant current pump. 0.1 g catalyst diluted with 0.4 g quartz sand was loaded into the stainless steel tube. Before measurements, the catalyst was reduced at 350 ºC for 1 h in a 10% H_2/Ar flow (30 mL min^{-1}). During the test, an aqueous solution of methanol (H_2O:CH_3OH = 2:1) at a rate of 0.1 mL min^{-1} was fed into a vaporizer. H_2 (20 mL min^{-1}) was also introduced into the vaporizer to carry the feed vapor into the reactor at atmospheric pressure. The products were analyzed online by a gas chromatograph equipped with a TCD detector.

Discussion on the particle size of active components

CuO and ZnO are the primary components for the fresh Cs-$C_yF_zZ_{1.0}$ catalysts (Fig. 1a). The absence of Fe_2O_3 suggests that Fe species is highly dispersed. After H_2 reduction treatment, Cu and Fe_3O_4 appear (Fig. 1b). The peak intensity trends of Cu and Fe species are consistent with their relative contents. The particle sizes of Cu and Fe_3O_4 were obtained by XRD (see Table 1). However, the Cu particle sizes over Cs-$C_{0.2}F_{1.0}Z_{1.0}$ and Cs-$C_{0.2}F_{1.0}Z_{1.0}$ are lacking because the content of Cu is low and the diffraction peak of Cu (111) is covered by Fe_3O_4 (400). But we can speculate the Cu size follows an order Cs-$C_{0.2}F_{1.0}Z_{1.0}$＜Cs-$C_{0.5}F_{1.0}Z_{1.0}$＜Cs-$C_{0.8}F_{1.0}Z_{1.0}$ according to H_2-TPR results (Fig. S1).

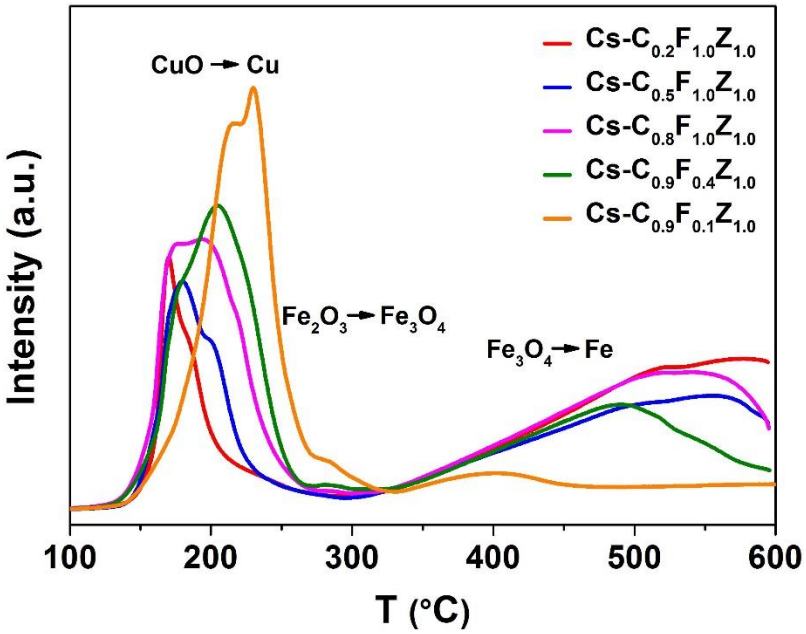

Fig. S1. H_2-TPR results of fresh Cs-$C_yF_zZ_{1.0}$ catalysts.

The reduction peak in the temperature range of 150-300 ºC is assigned to the reduction of CuO to metallic Cu along with Fe_2O_3 to Fe_3O_4.[1-4] And the broad reduction peak at above 300 ºC is ascribed to continuous reduction of Fe_3O_4 to metallic Fe.[1-4] With the increase of Cu/Fe molar ratio, the reduction peak area of CuO goes up while that of Fe_3O_4 decreases. Moreover, the reduction peak of CuO slightly shifts towards high temperature, verifying the increase in the particle size of CuO which is observed in the XRD patterns (Table 1).

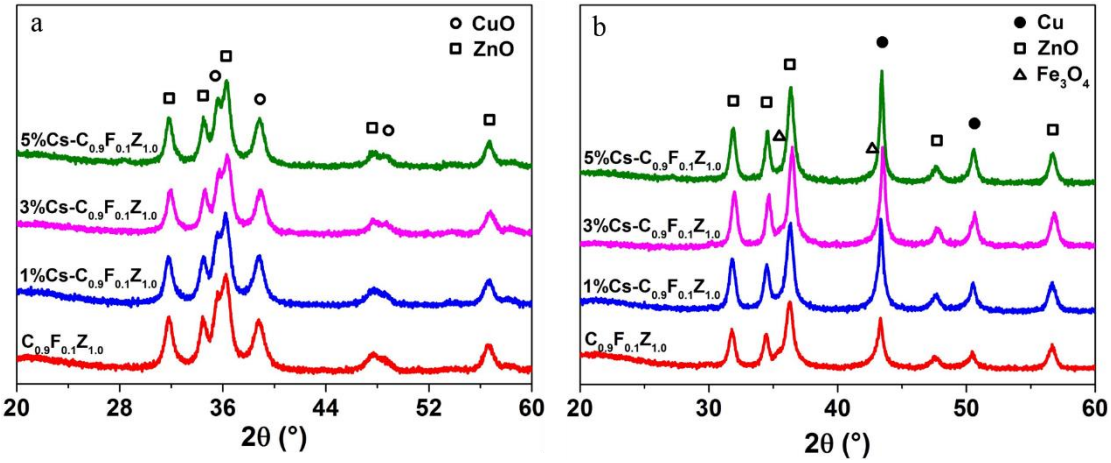

Fig. S2. XRD patterns over (a) fresh and (b) reduced x%Cs-$C_{0.9}F_{0.1}Z_{1.0}$ catalysts. Cu PDF#85-1326, CuO PDF#45-0937, ZnO PDF#79-2205, Fe_3O_4 PDF#75-1372.

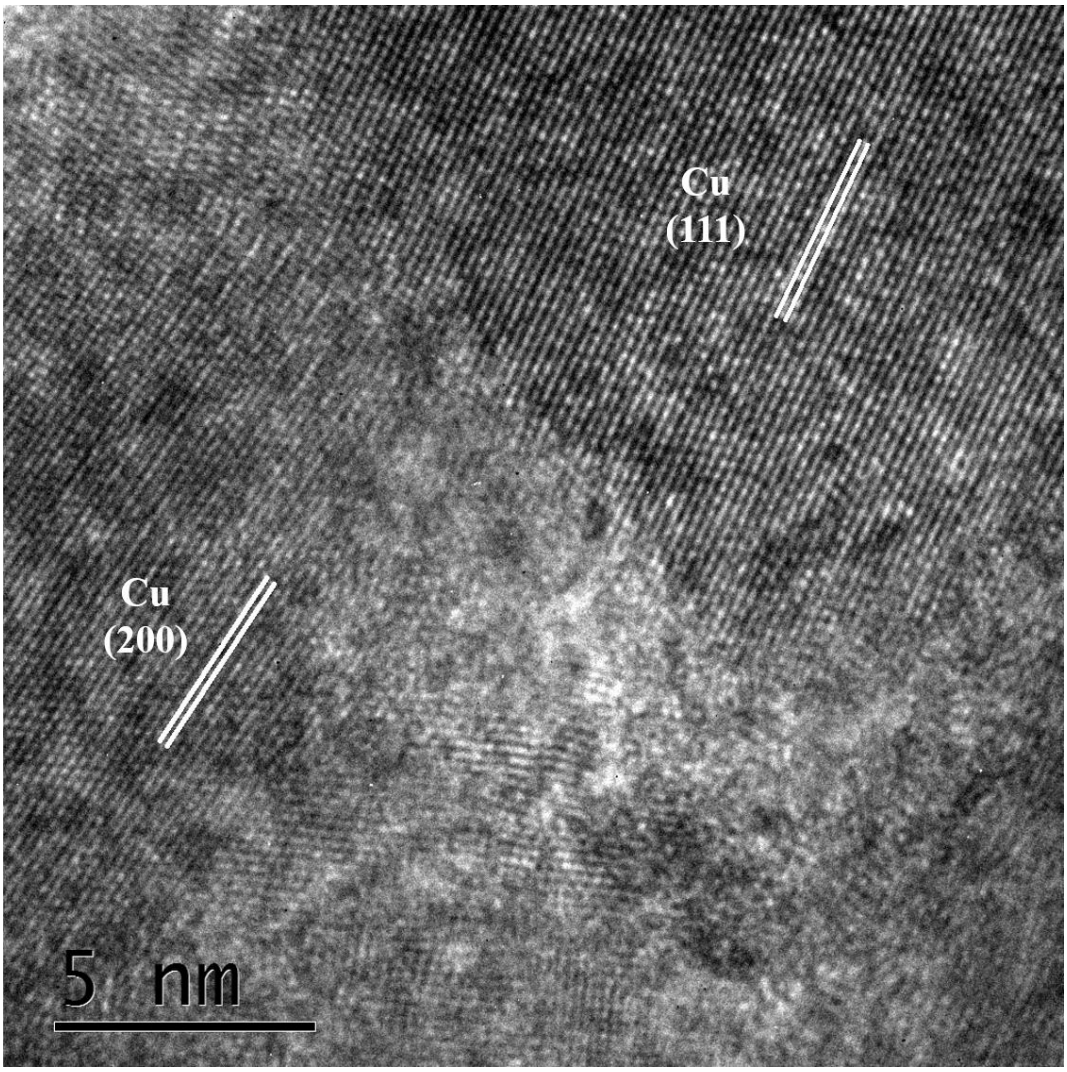

Fig. S3. HRTEM image of reduced Cs-$C_{0.8}F_{1.0}Z_{1.0}$ catalyst.

Table S1. Particle sizes of Cu/CuO and ZnO in fresh and reduced x%Cs-$C_{0.9}F_{0.1}Z_{1.0}$ catalysts calculated by the Scherrer formula.

Catalyst	Fresh		Reduced	
	d_{CuO} (nm)	d_{ZnO} (nm)	d_{Cu} (nm)	d_{ZnO} (nm)
$C_{0.9}F_{0.1}Z_{1.0}$	8.7	12.3	22.6	18.1
1%Cs-$C_{0.9}F_{0.1}Z_{1.0}$	9.5	12.6	25.0	16.8
3%Cs-$C_{0.9}F_{0.1}Z_{1.0}$	10.2	13.7	28.9	18.5
5%Cs-$C_{0.9}F_{0.1}Z_{1.0}$	10.2	14.4	31.6	17.9

Table S2. The amount of H_2 desorption over x%Cs-$C_{0.9}F_{0.1}Z_{1.0}$ catalysts.

Sample	H_2 desorption (umol g^{-1})			Total H_2 desorption (umol g^{-1})
	α	β	γ	
$C_{0.9}F_{0.1}Z_{1.0}$	25.3	101.5	60.4	187.2
1%Cs-$C_{0.9}F_{0.1}Z_{1.0}$	50.8	99.7	36.6	187.1
3%Cs-$C_{0.9}F_{0.1}Z_{1.0}$	60.6	84.1	43.1	187.8
5%Cs-$C_{0.9}F_{0.1}Z_{1.0}$	95.6	68.2	24.4	188.2

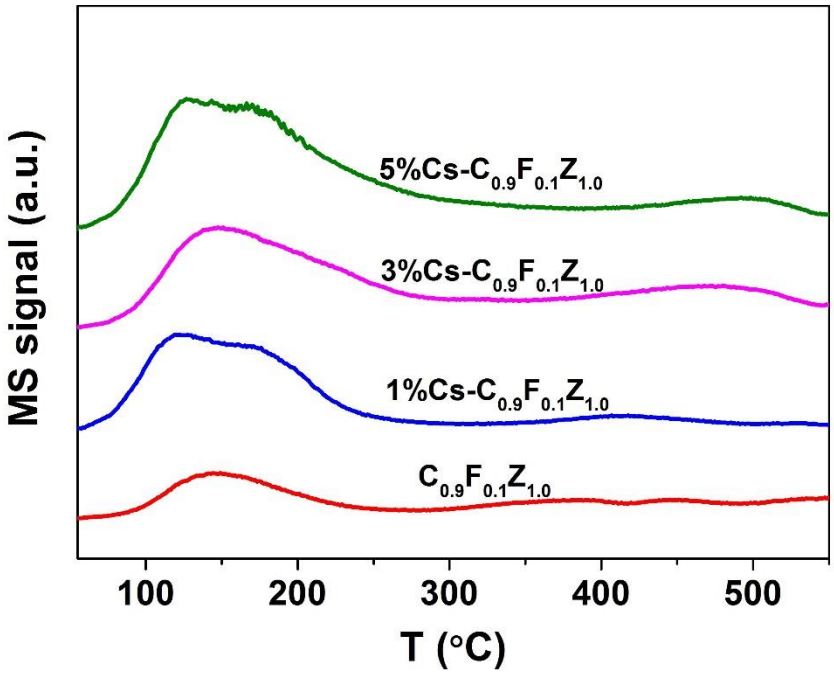

Fig. S4. CO_2-TPD-MASS results over x%Cs-$C_{0.9}F_{0.1}Z_{1.0}$ catalysts.

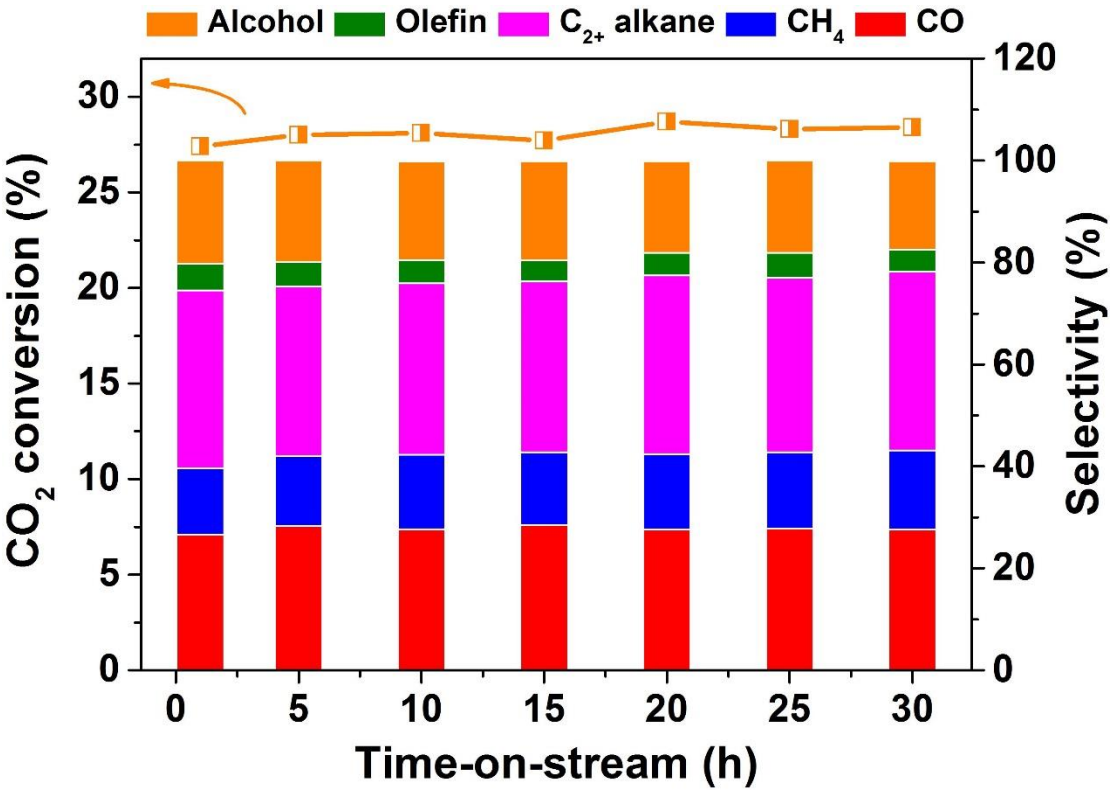

Fig. S5. Time-on-stream test of the Cs-$C_{0.8}F_{1.0}Z_{1.0}$ catalyst in CO_2 hydrogenation. Reaction conditions: 200 mg catalyst diluted by 400 mg quartz sand; H_2/CO_2 = 3:1; 5 MPa; 15 mL min^{-1}; 310 ºC.

Table S3. Comparison of HAS activity over Cs-$C_{0.8}F_{1.0}Z_{1.0}$ with some advanced catalysts in the literature in HAS from CO_2 hydrogenation.

Catalyst	Reactor	Reaction conditions	X_{CO2}[a] (%)	S_{HA}[b] (%)	S_{VP}[c] (%)	Y_{HA}[d] (%)	STY_{HA} (mmol g_{cat}^{-1} h^{-1})	W_{HA}[e] (%)	Ref.
Pt/Co_3O_4	Tank	20 mg, water/DMI, 8 MPa, 200 ºC	-	29.3	34.0	-	0.42	82.5	5
Pt/Co_3O_4-m	Fixed-bed	6000 h^{-1}, 2 MPa, 200 ºC	≈ 11	≈ 23	≈ 56	≈ 5.1	0.75	≈ 41.8	6
$CoAlO_x$	Tank	20 mg, water, 4 MPa, 140/200 ºC	-	92.1/88.9 (ethanol)	-	-	0.44/0.89 (ethanol)	-	7
$CuZnFe_{0.5}K_{0.15}$	Fixed-bed	5000 h^{-1}, 6 MPa, 300 ºC	42.3	31.9 (wt%)	-	13.5 (wt%)	0.17 (g mL_{cat}^{-1} h^{-1})	87.1	1
RhFeLi-TiO_2	Fixed-bed	6000 h^{-1}, 3 MPa, 250 ºC	15.7	31.3 (ethanol)	33.5	4.9 (ethanol)	1.32 (ethanol)	93.2 (ethanol)	8
Rh-0.3VO_x/MCM-41	Fixed-bed	6000 h^{-1}, 3 MPa, 250 ºC	12.1	24.1 (ethanol)	41.9	2.9 (ethanol)	1.04 (ethanol)	49.4 (ethanol)	9
Cu/Co_3O_4-2h	Fixed-bed	36000 h^{-1}, 3 MPa, 250 ºC	13.9	15.2 (ethanol)	55.6	2.1	1.87 (ethanol)	-	10
Na-Co/SiO_2	Fixed-bed	4000 h^{-1}, 5 MPa, 250 ºC	18.8	8.7	33.4	1.6	-	87.5	11
Cs-$C_{0.8}F_{1.0}Z_{1.0}$	Fixed-bed	4500 h^{-1}, 5 MPa, 330 ºC	36.6	19.8	67.6	7.2	1.47 (ethanol 1.12)	93.8	This work

[a] CO_2 conversion.
[b] Alcohol selectivity.
[c] Valuable products (e.g. alcohols and C_{2+} hydrocarbons) selectivity.
[d] HA yield.
[e] Weight percent of HA in total alcohol.

Discussion on the effect of BET surface area

The surface area (SA) is an important factor for the activity of a catalyst. The physicochemical properties of our Cs-$C_yF_zZ_{1.0}$ catalysts are showed in Table 1. All catalysts have similar BET surface area and porosity. We then try to correlate catalytic activity with SA. From Fig. S6, there is no linear relevance between CO_2 conversion and BET SA. So, we can conclude that the CO_2 conversion is not directly determined by the surface area in our catalysis system.

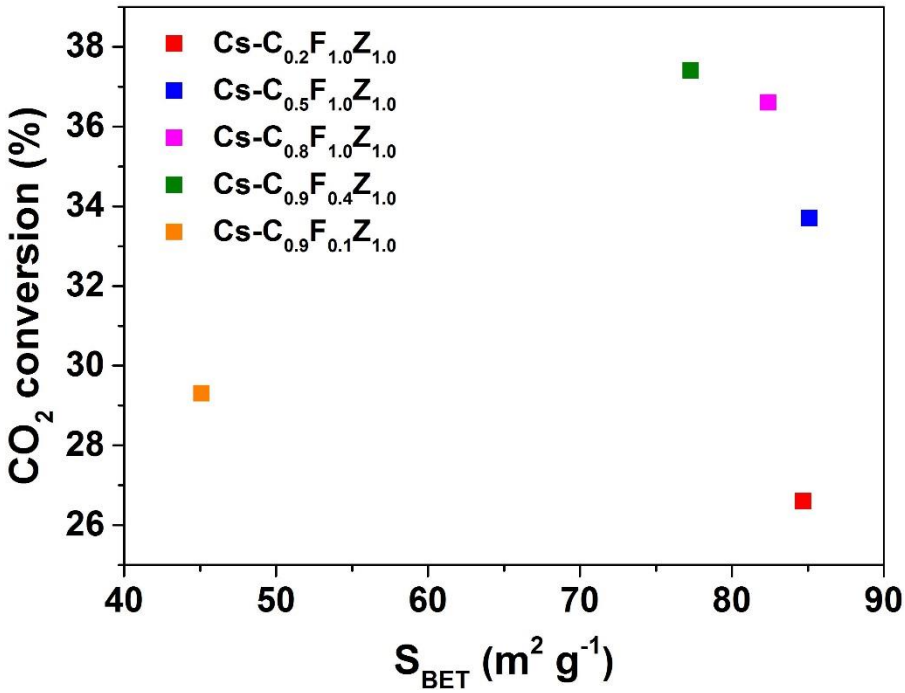

Fig. S6. CO_2 conversion at 330 ºC as a function of BET surface area of Cs-$C_yF_zZ_{1.0}$ catalysts.

Discussion on the effect of particle size

The particle sizes of active Cu and Fe species are also an important factor for catalytic performance. It is reported that high HA selectivity is obtainable if Cu is around 10 nm in size and Fe is moderately aggregate for CO hydrogenation over CuFe catalysts.[12] However, in this work, the trend of catalytic performance is not monotonous with particle size of individual species, which rules out the effect of particle size (Fig. S7).

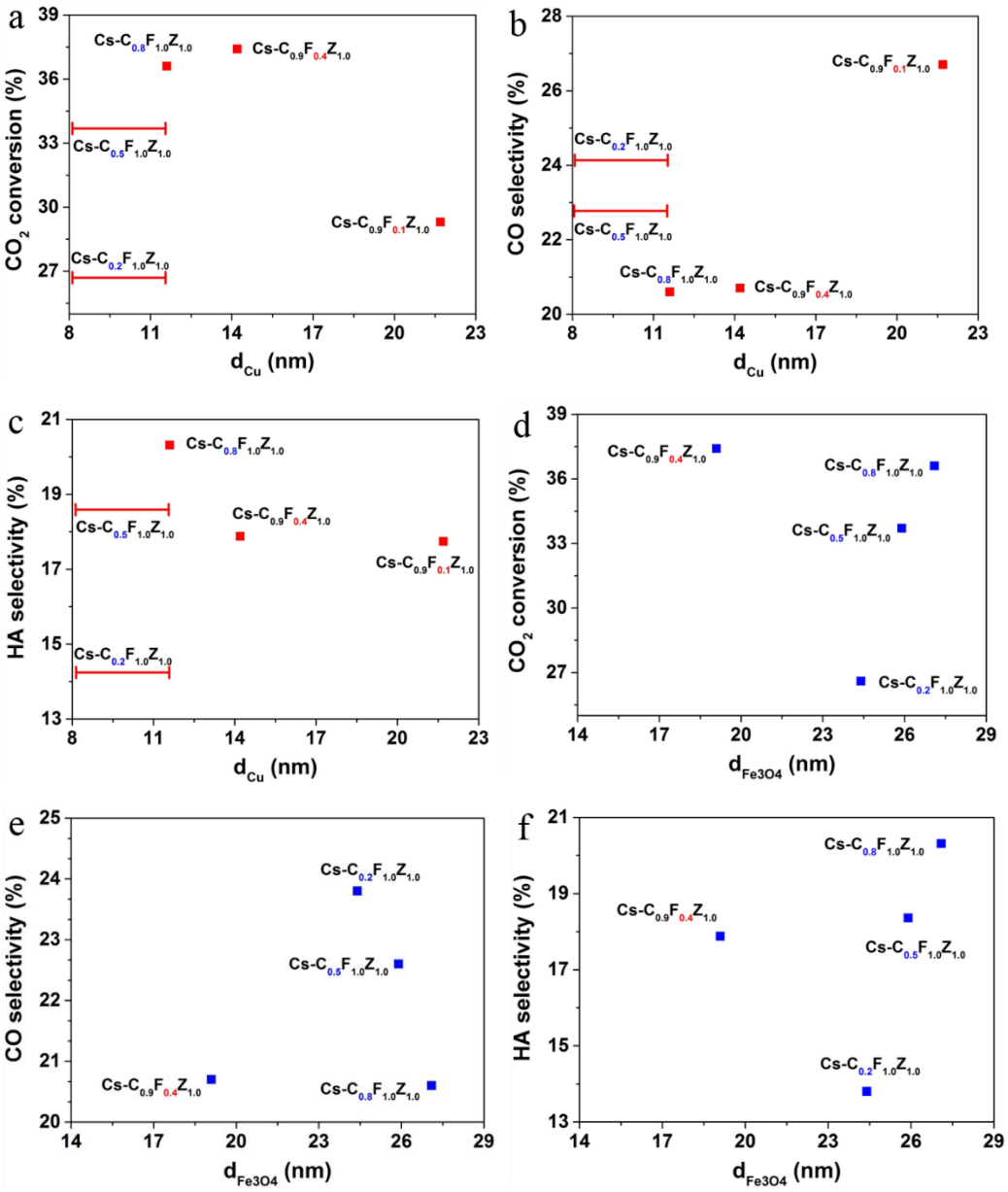

Fig. S7. Correlations between catalytic performance (CO_2 conversion, CO and HA selectivity) at 330 ºC and particle size of Cu (a, b and c) and Fe_3O_4 (d, e and f).

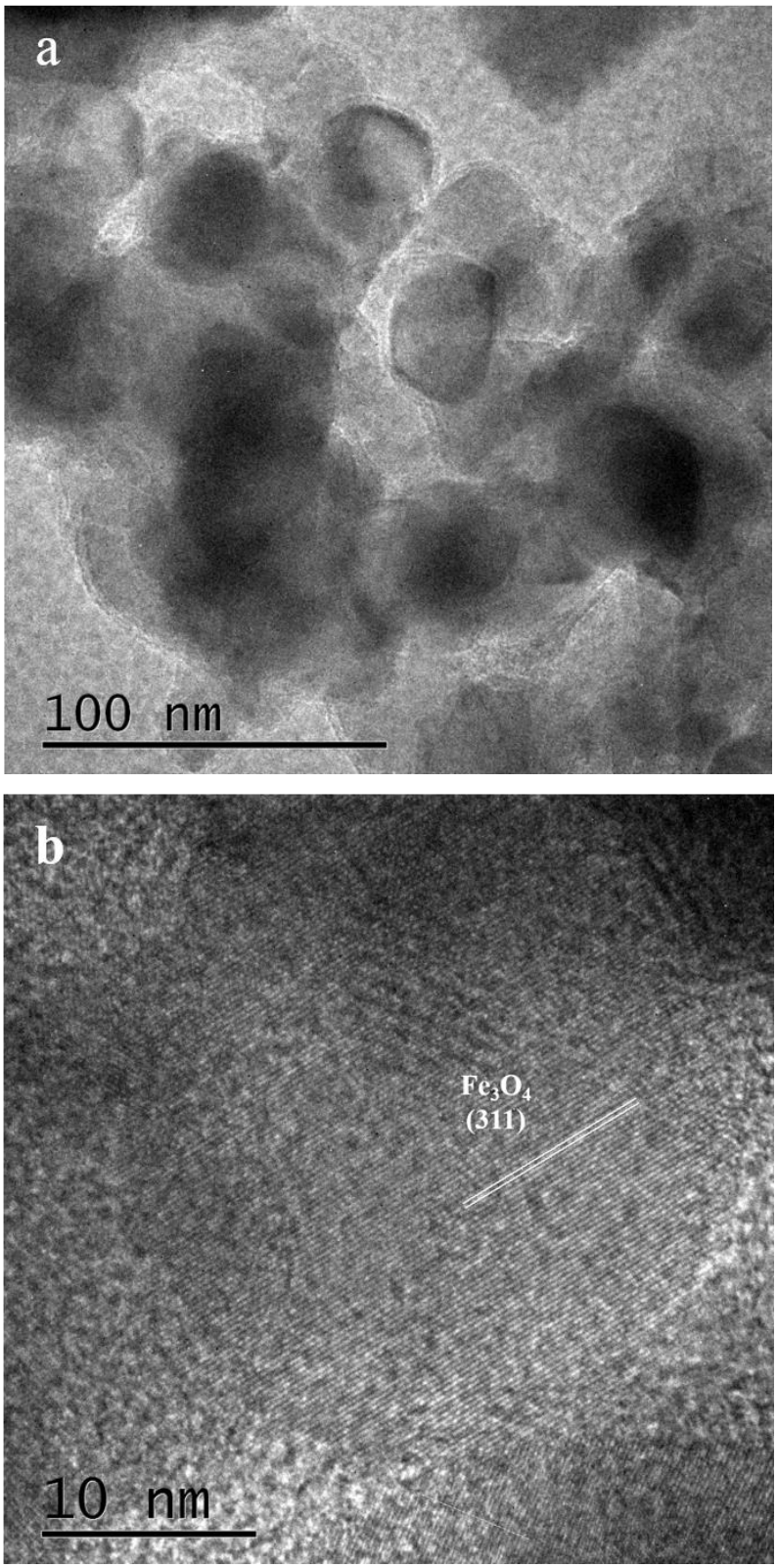
a
100 nm
b
Fe_3O_4
(311)
10 nm

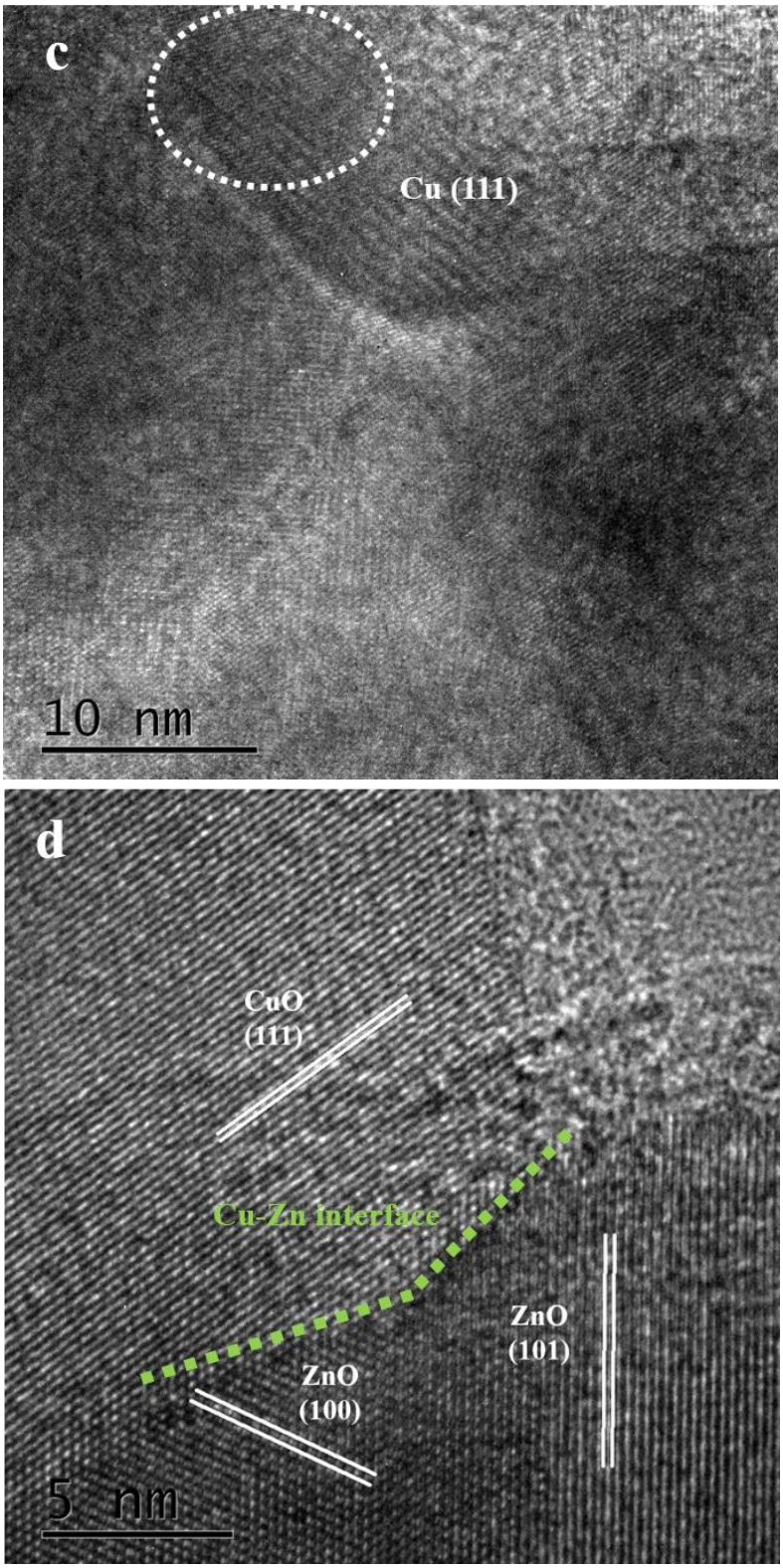

Fig. S8. TEM images of Cs-$C_{0.8}F_{1.0}Z_{1.0}$ catalyst after TOS test.

Table S4. Particle size of Cu, ZnO and Fe_3O_4 in the Cs-$C_{0.8}F_{1.0}Z_{1.0}$ catalyst after different treatments calculated by the Scherrer formula.

Catalyst	d_{Cu} (nm)	d_{ZnO} (nm)	d_{Fe3O4} (nm)
Spent catalyst pre-reduced with H_2/Ar	30.1	45.9	44.6
Spent catalyst pre-reduced with diluted syngas	31.2	39.4	75.4
After TOS	33.1	51.4	44.1

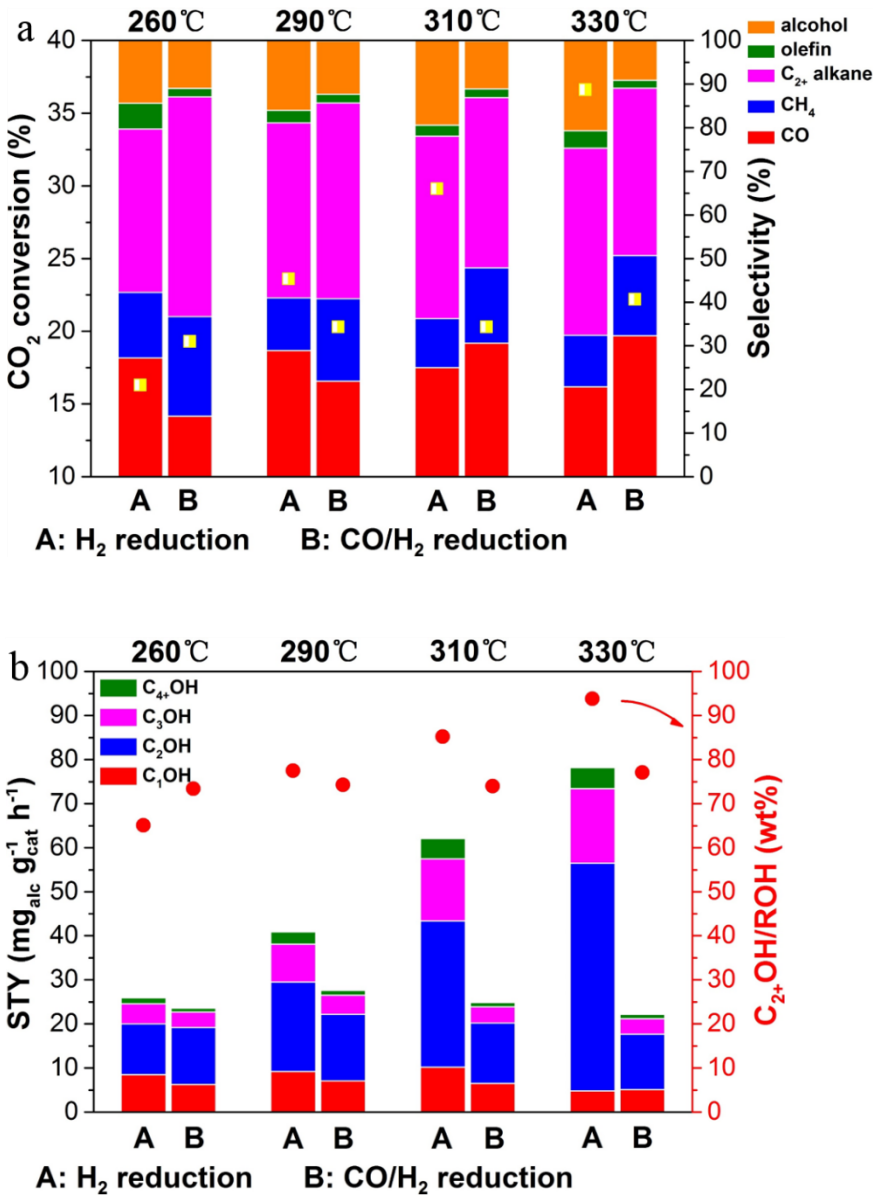

Fig. S9. Comparison of HAS activities over Cs-$C_{0.8}F_{1.0}Z_{1.0}$ reduced by different gas flows: 10% H_2/Ar reduction (A) and diluted syngas reduction (B). (a) CO_2 conversion (yellow square) and product distribution (CO, CH_4, C_{2+} alkane, olefin and alcohol, in all carbon products); (b) STY of different alcohols and C_{2+}OH/ROH weight contents (red circle). Reaction conditions: catalyst 200 mg and quartz sand 400 mg; H_2/CO_2 = 3:1; 5 MPa; 15 mL min^{-1}; 260-330 ºC.

Discussion on the effect of reduction conditions

We also investigated the influence of pre-reduction conditions on the activity of Cs-$C_{0.8}F_{1.0}Z_{1.0}$. The catalyst reduced by H_2/Ar is denoted as Catalyst A. The reference catalyst was treated by diluted syngas at 350 ºC for 5 h, denoted as Catalyst B. Fig. S9 shows that, as the reaction temperature is raised from 260 ºC to 310 ºC, the CO_2 conversion over Catalyst A is significantly enhanced while that over Catalyst B shows just a slight increasing trend. The selectivity and STY of total alcohols or $C_{2+}OH$ over Catalyst B are much lower than those over Catalyst A. This reveals that H_2/Ar reduction is preferable and much better than syngas reduction for our Cs-$C_{0.8}F_{1.0}Z_{1.0}$ catalysts.

To rationalize the poor activity of Catalyst B, we next compared the particle size of Cu, Fe and Zn species in Catalyst A and Catalyst B. As seen in Table S4, after syngas reduction, the agglomeration of Fe_3O_4 phase is severe (75.4 nm) when compared with that by H_2 reduction (44.6 nm) while ZnO and Cu are almost the same. This is probably because syngas has a stronger reducing activity than H_2/Ar, which causes a severe sintering of Fe_3O_4. Moreover, there is still no diffraction peaks of iron carbide for the spent Catalyst B (Fig. S10). So the poor activity of Catalyst B results from severe sintering of Fe species and thus disfavoring the formation of abundant copper-iron carbide interfaces. By contrast, a mild reduction treatment (H_2/Ar and the following *in-situ* reaction condition) is beneficial to the formation of copper-iron carbide interfaces as active sites for HAS.

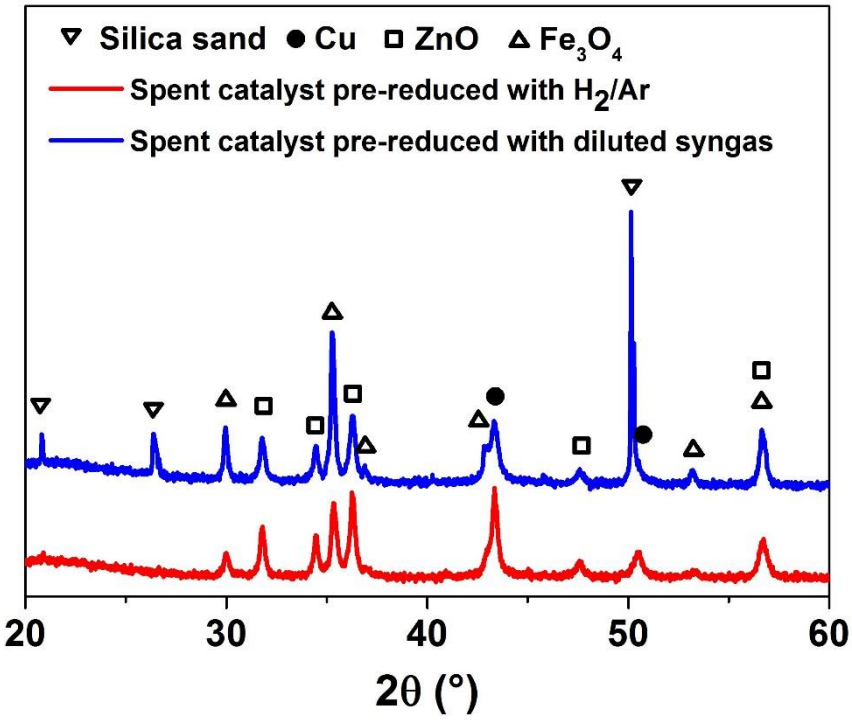

Fig. S10. PXRD patterns over spent Cs-$C_{0.8}F_{1.0}Z_{1.0}$ catalyst pre-reduced by H_2/Ar or diluted syngas. Cu PDF#85-1326, ZnO PDF#79-2205, Fe_3O_4 PDF#75-1372.

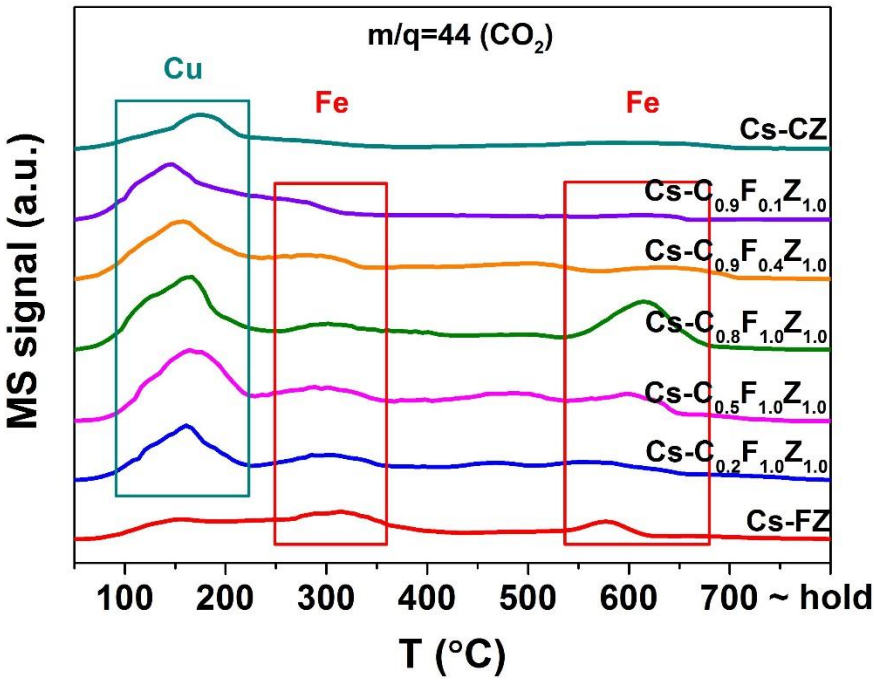

Fig. S11. H_2-TPSR-MS results of desorbed CO_2 over CO pre-adsorbed Cs-$C_yF_zZ_{1.0}$ catalyst.

Table S5. Proportion (A%) of desorbed CO, CO_2 and CH_4 species in all desorbed carbon-based molecules (CO_2, CO and CH_4) calculated by MS peak areas and catalytic performance over different Cs-$C_yF_zZ_{1.0}$ catalysts.

Sample	A_{CO}%[a] (%)	A_{CO2}% (%)	A_{CH4}% (%)	S_{HC}[b] (%)	S_{CO} (%)	S_{HA} (%)	STY_{HA} (mg g_{cat}^{-1} h^{-1})
Cs-$C_{0.2}F_{1.0}Z_{1.0}$	16.9	26.7	56.4	62.4	23.8	13.8	36.2
Cs-$C_{0.5}F_{1.0}Z_{1.0}$	22.6	32.3	45.1	58.7	22.6	17.9	64.5
Cs-$C_{0.8}F_{1.0}Z_{1.0}$	25.7	30.3	44.0	58.7	20.6	19.8	73.4
Cs-$C_{0.9}F_{0.4}Z_{1.0}$	34.1	28.8	37.1	61.2	20.7	17.4	65.5
Cs-$C_{0.9}F_{0.1}Z_{1.0}$	39.5	29.5	31.0	54.7	26.7	17.2	51.7

[a] A% stands for the proportion of MS peak area for specific species.

[b] Product selectivity.

As for all Cs-$C_yF_zZ_{1.0}$ catalysts, CO_2 desorption shows three peaks (peak α at 150 ºC, β at 300 ºC and γ at 600 ºC). As a reference, Cs-CZ (without Fe) exhibits good WGS activity at low temperature region while Cs-FZ (without Cu) shows relatively weak CO_2 desorption at 300 ºC and 600 ºC (Fig. S11). So we can conclude that Cu sites mainly contribute to α while Fe species contribute to β and γ. The CO_2 desorption capability can reflect the RWGS ability in our real condition. With the increase in Cu/Fe molar ratio, the peak intensity of CO_2 increases first and then decreases (see Table S5), implying the synergistic effect between Cu and Fe species.

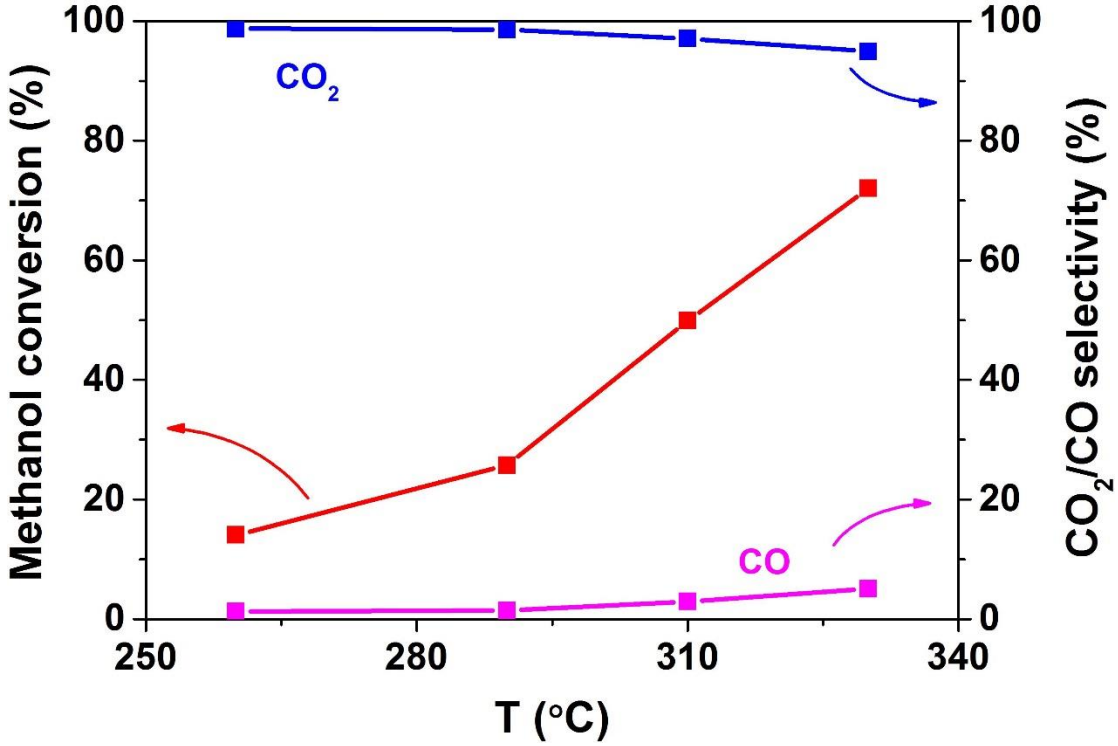

Fig. S12. Catalytic performance (methanol conversion and CO_2/CO selectivity) of the Cs-$C_yF_zZ_{1.0}$ catalyst. Reaction conditions: 100 mg catalyst diluted by 400 mg quartz sand; methanol/water = 1:2, 0.1 mL min^{-1}; carrier gas H_2 flow=20 mL min^{-1}; 260-330 ºC.

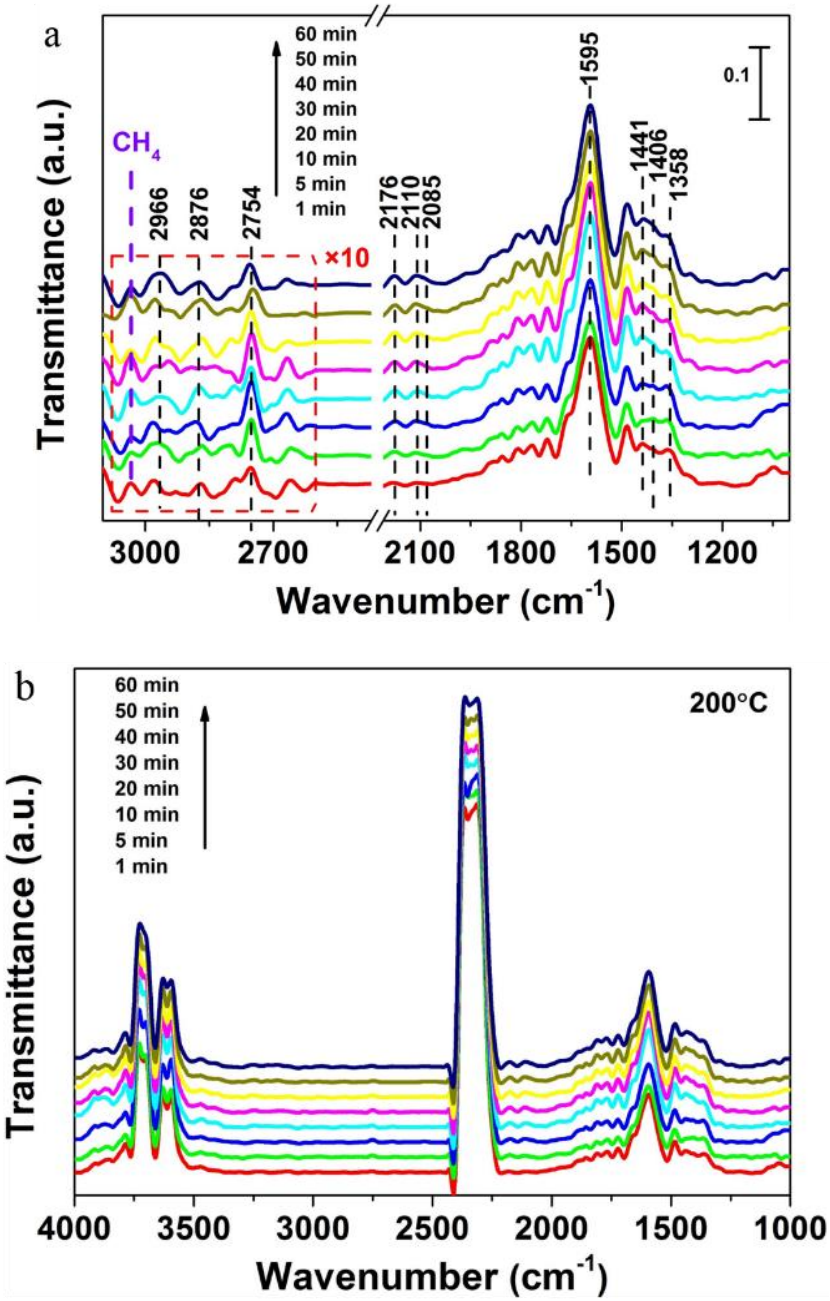

Figure S13. (a) In situ DRIFTS spectra and (b) full-range (1000 ~ 4000 cm^{-1}) spectra of the CO_2+H_2 reaction over Cs-$C_{0.5}F_{1.0}Z_{1.0}$ catalyst taken under 0.3 MPa CO_2/H_2 flow at 200 ºC.

The characteristic band of gaseous CH_4 is at ~3016 cm^{-1}. Indeed, the small peak at 3025 cm^{-1} is likely assigned to gaseous CH_4 (Fig. S13a). As for the other alkyl species, the characteristic bands are overlapped with carbonate and bicarbonate species in the range of 1300-1500 cm^{-1}. The bands for CO_2 overtones and hydroxyl are displayed in the range of 3100-4000 cm^{-1} (Fig. S13b).

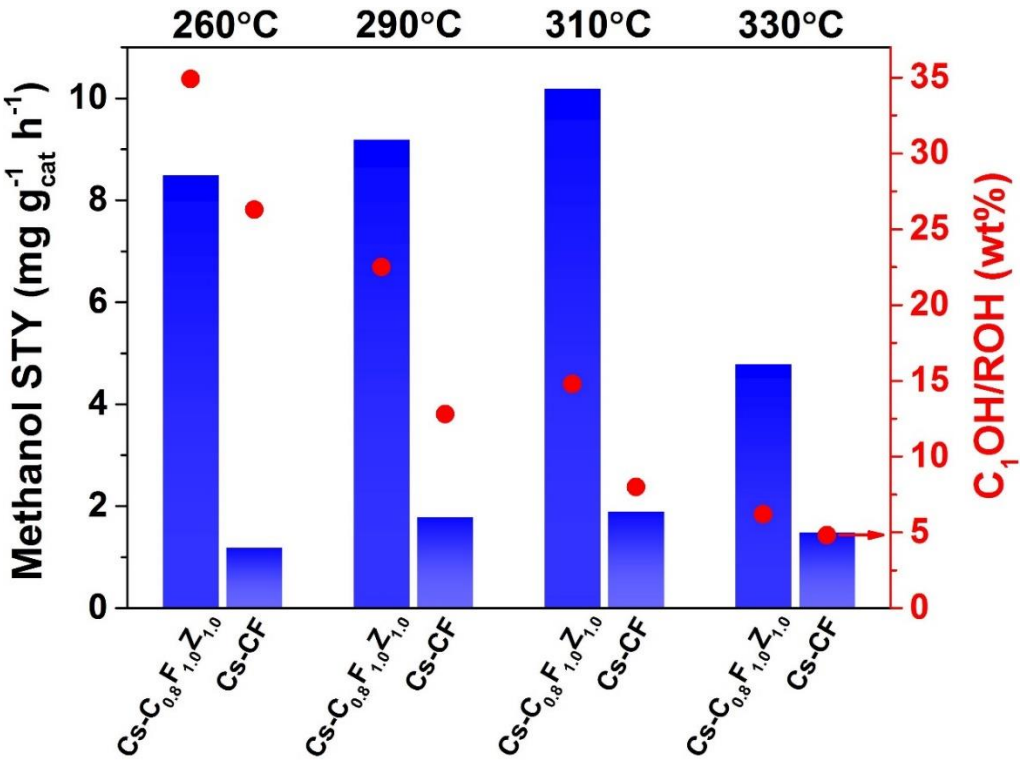

Fig. S14. Methanol STY (blue bar chart) and its weight percent in total alcohols (red circle) over Cs-$C_{0.8}F_{1.0}Z_{1.0}$ and Cs-CF catalysts.

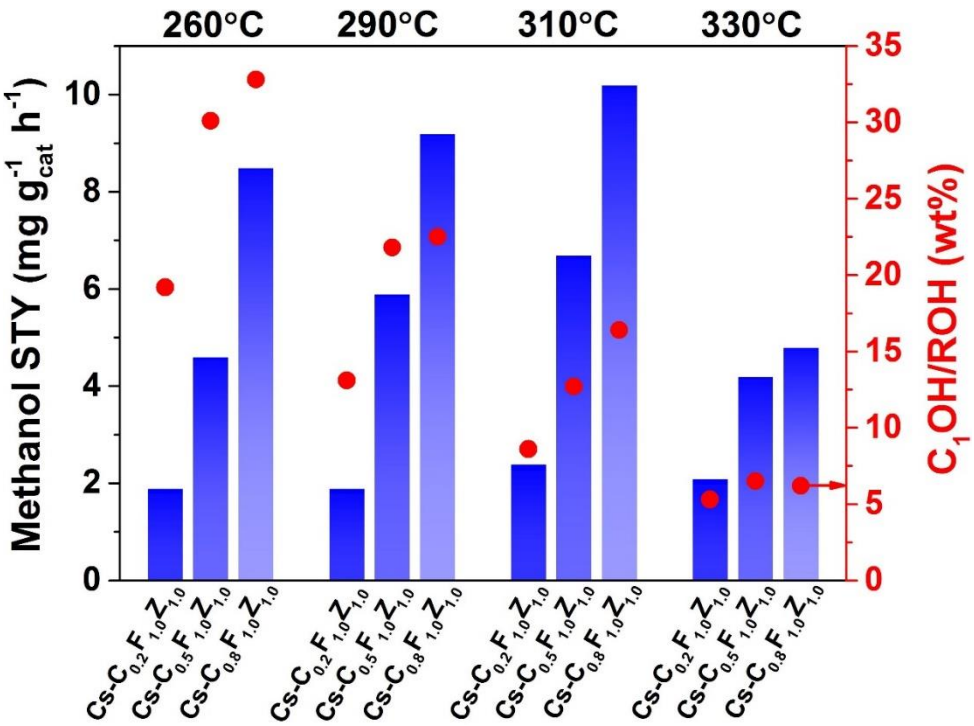

Fig. S15. Methanol STY (blue bar chart) and its weight percent in total alcohols (red circle) over Cs-$C_{0.2}F_{1.0}Z_{1.0}$, Cs-$C_{0.5}F_{1.0}Z_{1.0}$ and Cs-$C_{0.8}F_{1.0}Z_{1.0}$ catalysts.

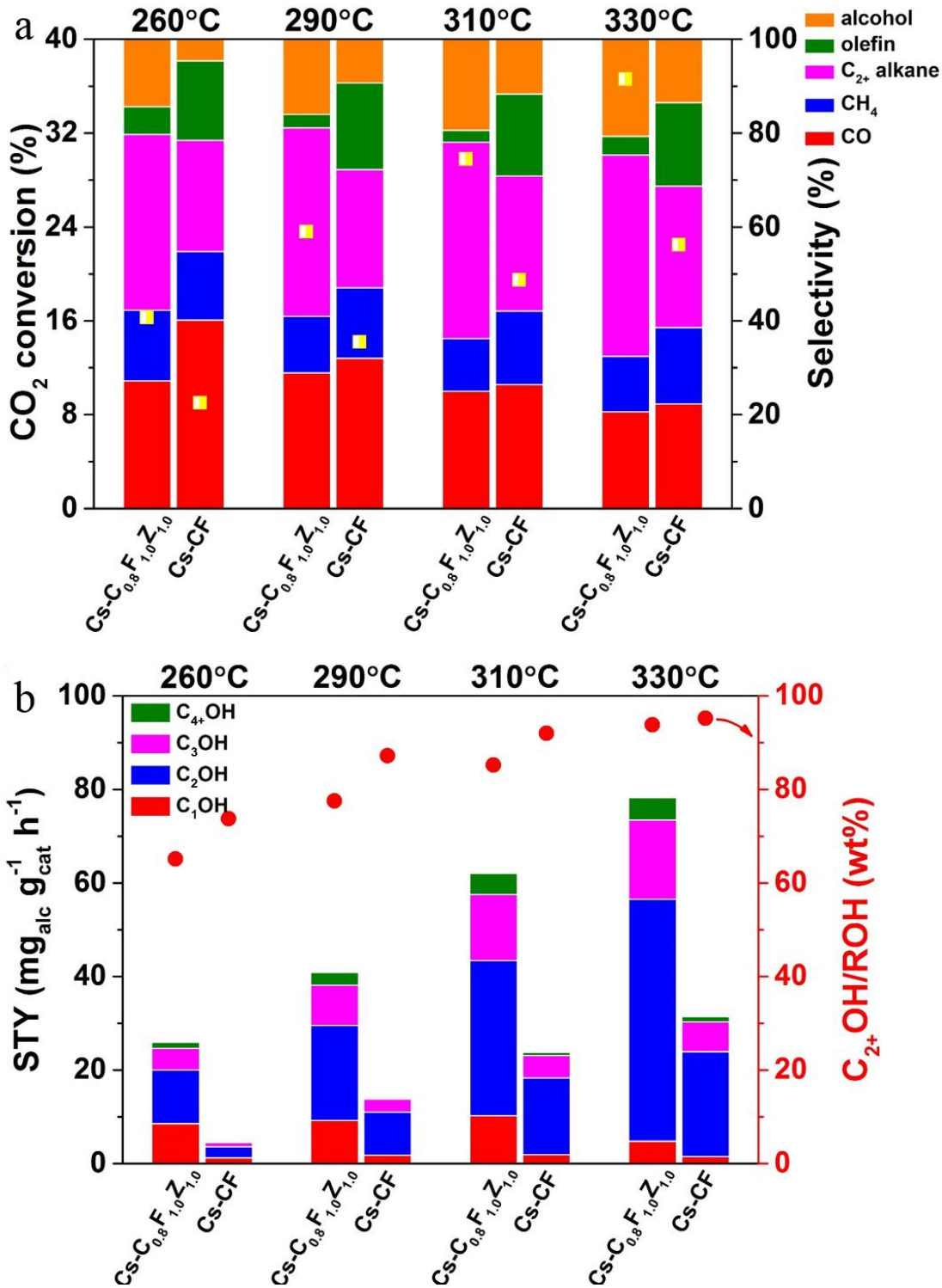

Fig. S16. Catalytic performance of Cs-CF and Cs-$C_{0.8}F_{1.0}Z_{1.0}$ catalysts. (a) CO_2 conversion (yellow square) and product selectivity (CO, CH_4, C_{2+} alkane, olefin and alcohol, in all carbon products), (b) STY of alcohols and C_{2+}OH/ROH selectivity (red circle). Reaction conditions: 200 mg catalyst and 400 mg quartz sand; H_2/CO_2 = 3:1; 5 MPa; 15 mL min^{-1}; 260-330 ºC.

Discussion on the effect of ZnO

As showed in Fig. S17, we can clearly see that the CuO and Cu particles would grow bigger without the protection of ZnO. Fe_3O_4 shows the similar results. Therefore, ZnO plays an important role in dispersing and stabilizing Cu and Fe species. Moreover, ZnO is a good partner to Cu. Cu-ZnO is a widely studied catalyst system for methanol synthesis as well as RWGS reaction.[13-18] The high RWGS activity of Cu-ZnO would provide a relatively high fraction of initial CO for tandem reaction. Theoretical calculations have shown that ZnO decoration can benefit the adsorption of O-anchored intermediates such as formate and acyl groups due to the oxophile property of Zn atoms.[16] In this content, Zn would promote the formation of oxy-compounds. ZnO is also a good hydrogen reservoir and hence increases the hydrogenation activity of Cu based catalysts, which can be further confirmed by the lower olefins/paraffin ratio over Cs-$C_{0.8}F_{1.0}Z_{1.0}$ (Fig. S16).[18,19]

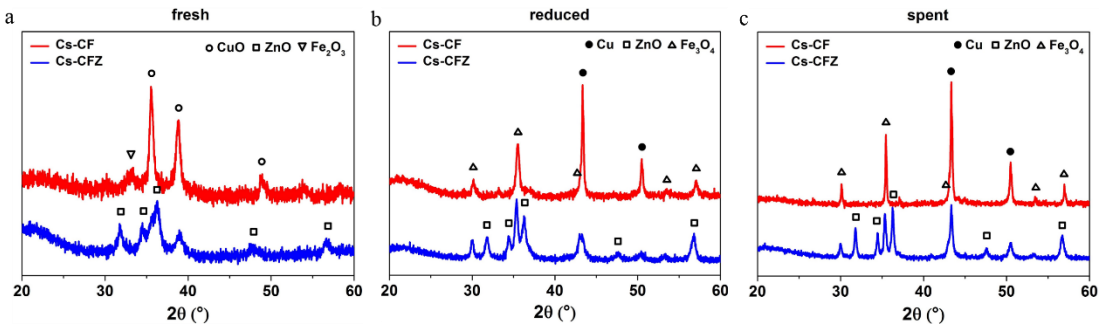

Fig. S17. XRD patterns over (a) fresh, (b) reduced and (c) spent Cs-CF and Cs-CFZ catalysts. Cu PDF#85-1326, CuO PDF#45-0937, ZnO PDF#79-2205, Fe3O4 PDF#75-1372.

References

(1) Li, S. G.; Guo, H. J.; Luo, C. R.; Zhang, H. R.; Xiong, L.; Chen, X. D.; Ma, L. L. Effect of Iron Promoter on Structure and Performance of K/Cu-Zn Catalyst for Higher Alcohols Synthesis from CO_2 Hydrogenation. *Catal. Lett.* **2013**, 143, 345-355.

(2) Han, X. Y.; Fang, K. G.; Zhou, J.; Zhao, L.; Sun, Y. H. Synthesis of Higher Alcohols over Highly Dispersed Cu-Fe Based Catalysts Derived from Layered Double Hydroxides. *J. Colloid Interface Sci.* **2016**, 470, 162-171.

(3) Ding, M. Y.; Qiu, M. H.; Liu, J. G.; Li, Y. P.; Wang, T. J.; Ma, L. L.; Wu, C. Z. Influence of Manganese Promoter on Coprecipitated Fe-Cu Based Catalysts for Higher Alcohols Synthesis. *Fuel* **2013**, 109, 21-27.

(4) Gao, W.; Zhao, Y. F.; Liu, J. M.; Huang, Q. W.; He, S.; Li, C. M.; Zhao, J. W.; Wei, M. Catalytic Conversion of Syngas to Mixed Alcohols over CuFe-Based Catalysts Derived from Layered Double Hydroxides. *Catal. Sci. Technol.* **2013,** 3, 1324-1332.

(5) He, Z. H.; Qian, Q. L.; Ma, J.; Meng, Q. L.; Zhou, H. C.; Song, J. L.; Liu, Z. M.; Han, B. X. Water-Enhanced Synthesis of Higher Alcohols from CO_2 Hydrogenation over a Pt/Co_3O_4 Catalyst under Milder Conditions. *Angew. Chem. Int. Ed.* **2016**, 55, 737-741.

(6) Liu, B.; Ouyang, B.; Zhang, Y. H.; Lv, K. L.; Li, Q.; Ding, Y. B.; Li, J. L. Effects of Mesoporous Structure and Pt Promoter on the Activity of Co-Based Catalysts in Low-Temperature CO_2 Hydrogenation for Higher Alcohol Synthesis. *J. Catal.* **2018**, 366, 91-97.

(7) Wang, L. X.; Wang, L.; Zhang, J.; Liu, X. L.; Wang, H.; Zhang, W.; Yang, Q.; Ma, J. Y.; Dong, X.; Yoo, S. J.; Kim, J. G.; Meng, X. J.; Xiao, F. S. Selective Hydrogenation of CO_2 to Ethanol over Cobalt Catalysts. *Angew. Chem. Int. Ed.* **2018**, 57, 1-6.

(8) Yang, C. S.; Mu, R. T.; Wang, G. S.; Song, J. M.; Tian, H.; Zhao, Z. J.; Gong, J. L. Hydroxyl-mediated Ethanol Selectivity of CO_2 Hydrogenation. *Chemical Science* **2019**, 10, 3161-3167.

(9) Wang, G. S.; Luo, R.; Yang, C. S.; Song, J. M.; Xiong, C. Y.; Tian, H.; Zhao, Z. J.; Mu, R. T.; Gong, J. L. Active Sites in CO_2 Hydrogenation over Confined VO_x-Rh Catalysts. *Sci. Chi. Chem.* **2019**, 62, 1710-1719.

(10) Yang, C. S.; Liu, S. H.; Wang, Y. N.; Song, J. M.; Wang, G. S.; Wang, S.; Zhao, Z. J.; Mu, R. T.; Gong, J. L. The Interplay between Structure and Product Selectivity of CO_2 Hydrogenation. *Angew. Chem. Int. Ed.* **2019**, 58, 1-6.

(11) Zhang, S. N.; Liu, X. F.; Shao, Z. L.; Wang, H.; Sun, Y. H. Direct CO_2 Hydrogenation to Ethanol over Supported Co_2C Catalysts: Studies on Support Effects and Mechanism. *J. Catal.* **2020**, 382, 86-96.

(12) Luk, H. T.; Mondelli, C.; Mitchell, S.; Siol, S.; Stewart, J. A.; Ferré, D. C.; Pérez-Ramírez, J. Role of Carbonaceous Supports and Potassium Promoter on Higher Alcohols Synthesis over Copper-Iron Catalysts. *ACS Catal.* **2018**, 8, 9604-9618.

(13) Daza, Y. A.; Kuhn, J. N. CO_2 Conversion by Reverse Water Gas Shift Catalysis: Comparison of Catalysts, Mechanisms and Their Consequences for CO_2 Conversion to Liquid Fuels. *RSC Adv.* **2016**, 6, 49675-49691.

(14) Roy, S.; Cherevotan, A.; Peter, S. C. Thermochemical CO_2 Hydrogenation to Single Carbon Products: Scientific and Technological Challenges. *ACS Energy Lett.* **2018**, 3, 1938-1966.

(15) Artz, J.; Muller, T. E.; Thenert K. Sustainable Conversion of Carbon Dioxide: An Integrated Review of Catalysis and Life Cycle Assessment. *Chem. Rev.* **2018**, 118, 434-504.

(16) Behrens, M.; Studt, F.; Kasatkin, I.; Kuhl, S.; Havecker, M.; Abild-Pedersen, F.; Zander, S.; Girgsdies, F.; Kurr, P.; Kniep, B. L.; Tovar, M.; Fischer, R. W.; Norskov, J. K.; Schlogl, R. The Active Site of Methanol Synthesis over $Cu/ZnO/Al_2O_3$ Industrial Catalysts. *Science* **2012**, 336, 893-897.

(17) Kuld, S.; Thorhauge, M.; Falsig, H.; Elkjaer, C. F.; Helveg, S.; Chorkendorff, I.; Sehested, J. Quantifying the Promotion of Cu Catalysts by ZnO for Methanol Synthesis. *Science* **2016**, 352, 969-974.

(18) Kattel, S.; Ramirez, P. J.; Chen, J. G. G.; Rodriguez, J. A.; Liu, P. Active Sites for CO_2 Hydrogenation to Methanol on Cu/ZnO Catalysts. *Science* **2017**, 355, 1296-1299.

(19) Cheng, K.; Zhou, W.; Kang, J. C.; He, S.; Shi, S. L.; Zhang, Q. H.; Pan, Y.; Wen, W.; Wang, Y. Bifunctional Catalysts for One-Step Conversion of Syngas into Aromatics with Excellent Selectivity and Stability. *Chem* **2017**, 3, 334-347.